**Proceedings Paper:**
Nguyen, YTH, McLernon, D orcid.org/0000-0002-5163-1975, Ghogho, M et al. (1 more author) (2019) Time-Frequency Distribution for Undersampled Non-stationary Signals using Chirp-based Kernel. In: 2018 5th NAFOSTED Conference on Information and Computer Science (NICS). NICS 2018: 5th NAFOSTED, 23 Nov - 24 Oct 2018, Ho Chi Minh city, Vietnam. IEEE , pp. 6-10. ISBN 978-1-5386-7983-8

https://doi.org/10.1109/NICS.2018.8606839

# Time-Frequency Distribution for Undersampled Non-stationary Signals using Chirp-based Kernel

1st Yen Thi Hong Nguyen
*Faculty of Electronics and Telecommunication Engineering,*
*Danang University of Science and Technology,*
Danang, Vietnam.
nthyen@dut.udn.vn

2nd Des McLernon
*School of Electronic and Electrical Engineering,*
*Leeds University,*
Leeds, UK.
D.C.Mclernon@leeds.ac.uk

3rd Mounir Ghogho
*Internaltional University of Rabat,*
Morocco.
m.ghogho@ieee.org

4th Ali Zaidi
*School of Electronic and Electrical Engineering,*
*Leeds University,*
Leeds, UK.
s.a.zaidi@leeds.ac.uk

***Abstract*—Missing samples and randomly sampled non-stationary signals give rise to artifacts that spread over both the time-frequency and the ambiguity domains. These two domains are related by a two-dimensional Fourier transform. As these artifacts resemble noise, the traditional reduced interference signal-independent kernels, which belong to Cohen's class, cannot mitigate them efficiently. In this paper, a novel signal-independent kernel in the ambiguity domain is proposed. The proposed method is based on three important facts. Firstly, any windowed non-stationary signal can be approximated as a sum of chirps. Secondly, in the ambiguity domain, any chirp resides inside certain regions, which just occupy half of the ambiguity plane. Thirdly, the missing data artifacts always appear along the Doppler axis where the chirps auto-terms do not appear. Therefore, we propose using a chirp-based fixed kernel on windowed non-stationary signals in order to remove half of the noise-like artifacts in the ambiguity domain and compensate for the missing data effect located along the Doppler axis. It is shown that our method outperforms other reduced interference time-frequency distributions.**

***Index Terms*—Reduced interference distribution, missing samples, non-stationary signal, time-frequency diforstribution, Cohen's class, chirp-based kernel.**

## I. Introduction

Non-stationary signals are ubiquitous in practice, and manifest themselves in speech, radar/sonar returns and biomedical signals, to name but a few. To analyze these signals, time-frequency distributions (TFDs) are widely used [1]–[7]. However, because non-stationary signals arise in many different applications, no single time-frequency (TF) estimation approach can be ideal in all cases. Therefore, this paper introduces a novel TFD, which can be classified into the reduced interference distribution (RID). It uses a kernel to attenuate the cross-terms between different components as well as those between the same components appearing in Wigner-Ville distribution (WVD). However, in contrast with traditional RIDs, which belong to the Cohen's class, the new kernel is applied for a windowed signal, not the whole signal, and it can partially combat missing samples. The kernel design is based on three facts. Firstly, chirp's auto-terms always reside in only a half of the ambiguity domain, which does not cover the Doppler axis. Thus, we can remove half of the ambiguity domain if the input signals are chirps. Additionally, according to [8] and [9], any non-stationary windowed signal can be approximated as a sum of chirps. So, for any non-stationary signal segment, we can cut half of the ambiguity plane. Moreover, the analysis of artifact distribution caused by missing samples shows that the artifact always appears along the Doppler axis. Thus, by filtering out the region along the Doppler axis, our chirp-based kernel gives improved time-frequency representation (TFR) in the case of incomplete data. So this paper is organized as follows. Section II presents the unsuitability of the traditional RIDs in the presence of missing data. Section III introduces the windowed chirp-based kernel. Section IV gives simulation results. Finally, conclusions are given in section V.

## II. THE TRADITIONAL RIDS AND THEIR UNSUITABILITY FOR INCOMPLETE DATA

For a complex-valued signal $(\tilde{s}(t))$ sampled with a period $T$, i.e., $s(n) = s(nT)$, the RID $D(n,k)$ is obtained by the two-dimensional Fourier transform of the product of the ambiguity function $A(p,b)$ and the kernel function $C(p,b)$ as follows:

$$D(n,k) = \sum_{p=-N/2}^{N/2-1} \sum_{b=-N}^{N-1} C(p,b)A(p,b)e^{j(-bk-pn)2\pi/N}, \quad (1)$$

with

$$A(p,b) = \sum_{n=0}^{N-1} s(n+\frac{b}{2})s^*(n-\frac{b}{2})e^{-j2\pi pn/N}, \quad (2)$$

where $k$ is the discrete frequency variable $k = 0, 1, ..., N-1$. In the ambiguity domain, most of the desired auto-terms are located at and around the origin, whereas the cross-terms reside at distant positions. The traditional kernel function acts as a low-pass filter in the ambiguity domain to preserve the

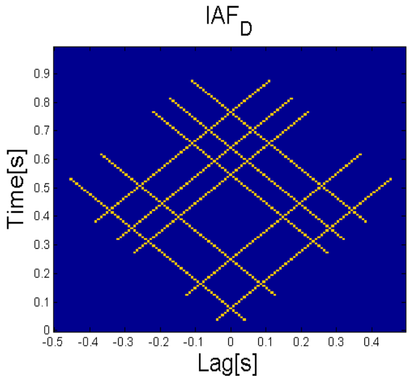


Fig. 1. The difference in the mask IAF with 5 random missing samples in the time domain.

auto-terms while suppressing the cross-terms. To maintain most of the desirable properties of the WVD, these kernels are required to satisfy some properties. The marginal property is one of them. It requires the kernel to be unity along lag and Doppler axis ($p = 0$ and $b = 0$). Some popular Cohen's class kernels are the Choi-Williams kernel [10], the Margenau-Hill kernel [11], the Rihaczek kernel [12] and the Born-Jordan kernel [13], etc. The kernel functions in the ambiguity domain of the afore-mentioned kernels are given in Table. I. According

TABLE I
SOME SIGNAL-DEPENDENT DISTRIBUTION AND THEIR KERNELS

| **Distribution** | **Kernel $C(p, b)$** |
|---|---|
| Choi-Williams | $\exp(-p^2b^2/\sigma)$ |
| Margenau-Hill | $\cos(pb/2)$ |
| Rihaczek | $\exp(jpb/2)$ |
| Born-Jordan | $\mathrm{sinc}(\frac{1}{2}pb)$ |

to [14], the missing data artifacts always appear along the Doppler axis. For illustration, the difference in the mask IAF due to five random missing data samples in the time domain is plotted in Fig. 1 [15]. It is obvious from Fig. 1 that missing sample artifacts always locate along the Doppler axis. And so the traditional kernels, which satisfy the marginal property, do not mitigate the missing data artifacts along the Doppler axis. Moreover, since the missing samples noise-like effect spreads all over the ambiguity plane, the conventional RIDs with the low-pass filters allow the artifact near the origin to pass through. Thus, traditional RIDs are unsuitable for incomplete data.

## III. CHIRP-BASED KERNEL

### *A. Properties of Chirps in The TF Domain and in The Ambiguity Domain*

Consider a certain chirp with a chirp-rate $\alpha$ and an initial frequency $\beta$ as follows:

$$s(n) = \exp\left[j2\pi\left(\alpha\frac{n^2}{2F_s^2} + \beta\frac{n}{F_s}\right)\right], \tag{3}$$

where $F_s$ is the sampling frequency, $n$ is the discrete time index, $n = 0, 1, ..., \lfloor T/T_s \rfloor$, $T$ is the total observation time and $T_s = 1/F_s$ is the sampling period. Let $N$ be the length of the signal $N = \lfloor T/T_s \rfloor$. The corresponding instantaneous autocorrelation function is expressed as:

$$\begin{aligned} R_{ss}(n, b) &= s(n + \frac{b}{2})s^*(n - \frac{b}{2}) \\ &= \exp\left[j2\pi\left(\alpha\frac{nb}{F_s^2} + \beta\frac{b}{F_s}\right)\right]. \end{aligned} \tag{4}$$

The WVD of $s(n)$ is expressed as:

$$\begin{aligned} D(n, \omega) &= \sum_b R_{ss}(n, b)e^{-j\omega b} \\ &= \delta\left[\frac{\omega}{2\pi} - (\beta + \alpha\frac{b}{F_s})\right]. \end{aligned} \tag{5}$$

Thus, the instantaneous frequency of the chirp signal s(n) is:

$$F(n) = \alpha\frac{n}{F_s} + \beta. \tag{6}$$

Assume that the signal is sampled at the Nyquist rate, i.e. the sampling frequency is double the maximum frequency of the signal, $F_s = 2F_{\max}$. Because $F_{\max}$ is the maximum frequency of the signal, so $F(n) \leq F_{\max}$. The maximum frequency change in $(N/F_s)$ is thus $F_{\max}$. As the chirp-rate is the frequency change of a chirp in one second, the maximum chirp-rate is as follows:

$$|\alpha_{\max}| = F_{\max}\frac{F_s}{N}. \tag{7}$$

The chirp signal $s(n)$ is expressed in the ambiguity domain as follows:

$$\begin{aligned} A(\omega', b) &= \sum_n R_{ss}(n, b)e^{-jn\omega'} \\ &= \exp(j2\pi\beta\frac{b}{F_s})\delta(\frac{\omega'}{2\pi} - \alpha\frac{b}{F_s}), \end{aligned} \tag{8}$$

where $\omega'$ is the Doppler angular frequency. Now (8) shows that the AF of all chirps has a linear support that passes through the origin of the ambiguity plane. The chirp auto-term lies at a certain angle to the horizontal line which is determined by the chirp-rate. Furthermore, since the chirp-rate is inside the range of $[-F_{\max}F_s/N, F_{\max}F_s/N]$, the angle ($\phi$) between the slope of the chirp and the horizontal line in the ambiguity domain is also restricted. The chirp signal $s(n)$ in the ambiguity domain is plotted in Fig. 2. Based on Fig. 2, the slope between the chirp line and the horizontal line in the ambiguity domain is as follows:

$$\phi = \arctan\frac{\alpha/\delta_f}{1/\delta_b} = \arctan\frac{2\alpha N}{F_s^2}, \tag{9}$$

where $\delta_f = F_s/N$ is the frequency resolution and $\delta_b = 2/F_s$ is the lag resolution. From (7) and (9), on the possitive plane, $\phi$ is bounded as:

$$-\frac{\pi}{4} \leq \phi \leq \frac{\pi}{4}. \tag{10}$$

Similarly, on the negative lag plane:

$$\frac{3\pi}{4} \leq \phi \leq \frac{5\pi}{4}. \tag{11}$$

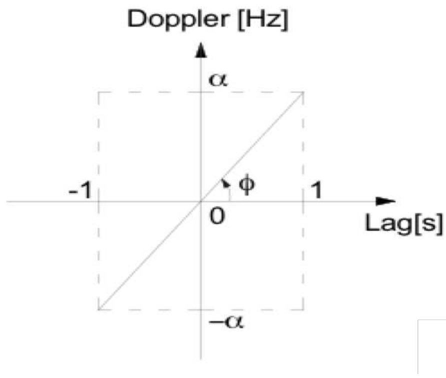


Fig. 2. A chirp signal in the ambiguity domain.

### B. Kernel Design for Chirp Signals

As discussed in section III-A, the auto-terms of chirps always locate inside $|\phi| \leq \pi/4$ and $3\pi/4 \leq \phi \leq 5\pi/4$. Thus we can filter out the rest, which corresponds to half of the ambiguity domain, to mitigate the effect of the cross-terms. And by removing half of the ambiguity domain, part of the noise-like effect caused by missing data is also attenuated. So based on this interpretation, we now design the chirp-based kernel. It is basically the Gaussian mask modified such that all components outside the region $|\phi| \leq \pi/4$ and $3\pi/4 \leq \phi \leq 5\pi/4$ are zero. A two-dimensional radially Gaussian kernel with a spread parameter $\sigma$ is given as [16]:

$$C(p, b) = e^{-\frac{p^2+b^2}{2\sigma^2}}. \tag{12}$$

The kernel is easily expressed in polar coordinates by using $r^2 = p^2 + b^2$ as the radius variable:

$$C(r, \phi) = e^{\frac{-r^2}{2\sigma^2}}. \tag{13}$$

So the proposed kernel is expressed as follows:

$$C(r, \phi) = \begin{cases} e^{-\frac{r^2}{2\sigma^2}}, & |\phi| \leq \pi/4 \quad \text{or} \quad 3\pi/4 \leq \phi \leq 5\pi/4 \\ 0, & \text{otherwise.} \end{cases} \tag{14}$$

The proposed kernel is illustrated in Fig. 3.

### C. Windowed Chirp-Based Kernel

According to [8], [9] and [17], the frequency law of any non-stationary windowed signal can be approximated as a sum of chirps. In another words, we can consider any windowed non-stationary signal as built from chirps and so we can apply the chirp-based kernel on the windowed non-stationary segments.

The TFDs of non-stationary signals using a chirp-based kernel proceeds as follows. The chirp-based kernel is first computed with the predefined window length $N_w$. At each

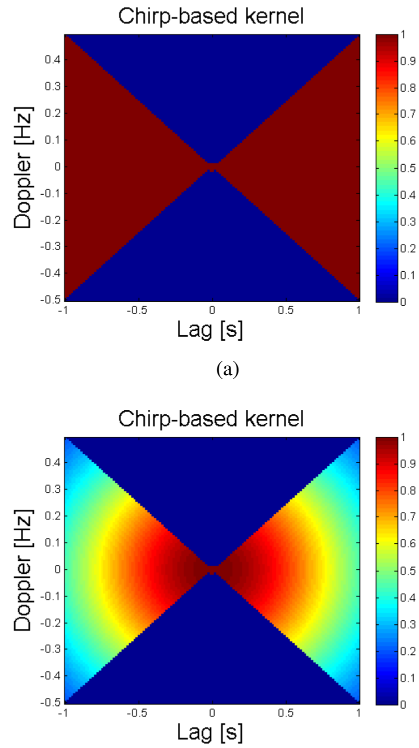


(a)

(b)

Fig. 3. The proposed kernel in the AF domain: (a) $\sigma = \infty$; (b) $\sigma = 50$.

time $n$, we compute the short-time ambiguity function (STAF) centered at time $n$, $AF(n; p, b)$. $AF(n; p, b)$ is given by [16]:

$$\begin{aligned} &AF(n; p, b) \\ &= \sum_u s^*(u - b/2) w^*(u - n - b/2) \\ &\quad s(u + b/2) w(u - n + b/2) e^{j2\pi up/N_w} \\ &= \sum_u IAF(n; u, b) w^*(u - n - b/2) \\ &\quad w(u - n + b/2) e^{j2\pi up/N_w}, \end{aligned} \tag{15}$$

where $w(u)$ is a symmetrical window function which is zero for $|u| > N_w/2$ and $u$ is the running time. The current-time slice of the TFR is computed as one slice (at time $n$ only) of the two-dimensional Fourier transform of the STAF-kernel product, expressed as follows:

$$\begin{aligned} &TFR(n, k) = \\ &\sum_p \sum_b A(n; p, b) C(n; p, b) e^{-j2\pi np/N_w} e^{-j2\pi bk/N_w}. \end{aligned} \tag{16}$$

## IV. SIMULATION RESULTS

This section evaluates the performance of the proposed RIDs, the windowed chirp-based kernel, when we have full and limited data. The proposed method is compared with two traditional RIDs, which are the Choi-Williams distribution and the Gaussian distribution. The WVD is also simulated here to see the TFRs without a kernel. Notice that all methods will be applied on sliding windowed signals. The resulting images are

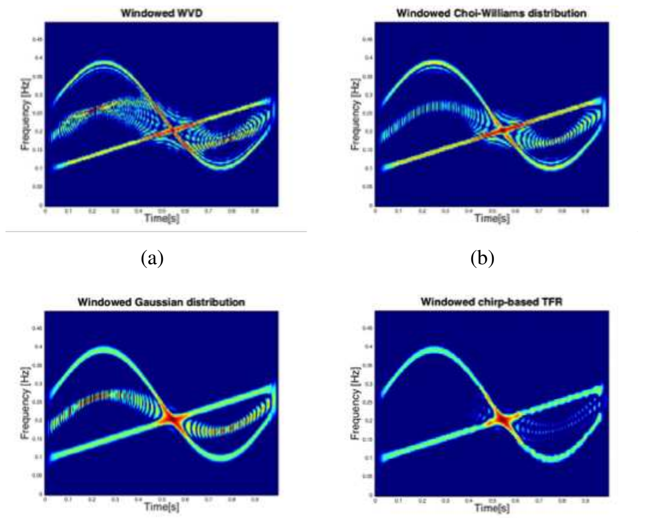


(a) (b) (c) (d)

Fig. 4. (a) WVD; (b) Choi-Williams distribution; (c) Gaussian distribution; (d) TFD obtained by the chirp-based kernel of the full signal in (17).

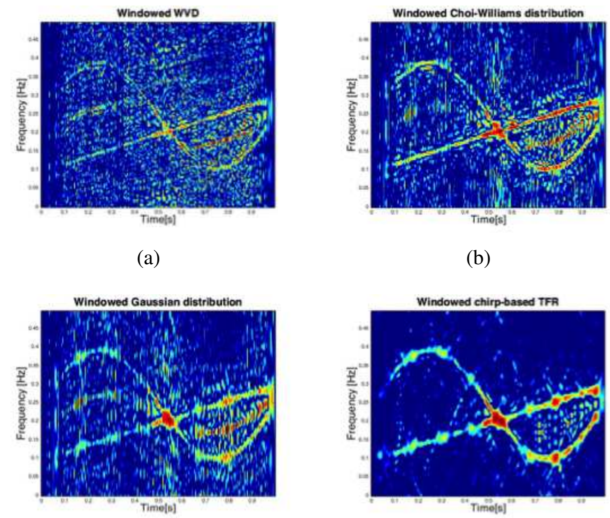


(a) (b) (c) (d)

Fig. 5. (a) WVD; (b) Choi-Williams distribution; (c) Gaussian distribution; (d) TFD obtained by the chirp-based kernel of the signal in (17) when 50% of data is missing.

normalized and transferred to the energy version to display. It is shown that the TFDs using the chirp-based kernel provide improved TF estimations when compared to conventional RIDs. In all plots, the frequency axis is normalized with respect to the sampling frequency $F_s$. The signal is sampled at the Nyquist rate, and then randomly shortened to 50% to create the incomplete data to be processed. The sampling frequency is $F_s$=256 Hz. The signals length is one second, or $N = F_s$ and $n = 0, ..., N-1$. The signal is corrupted by white Gaussian noise $v(n)$ and the signal-to-noise ratio (SNR) set to 30 dB. The example considers a multi-component signal as follows:

$$s(n) = \exp\left\{j(0.15F_s)\cos(2\pi\frac{n}{F_s}) + j2\pi(0.25F_s)\frac{n}{F_s}\right\} + \exp\left\{j2\pi\left[(0.1F_s)\frac{n}{F_s} + (0.2F_s)\frac{n^2}{2F_s^2}\right]\right\} + v(n). \tag{17}$$

Fig. 4 and Fig. 5 show the TF signatures of the full and the incomplete signals obtained by the proposed approach as well as other methods for comparison.

Fig. 4(a) and Fig. 5(a) show the windowed WVD. This method calculates the STAF, and the TFR is obtained by the two-dimensional Fourier transform. It can be seen that with no kernel, all cross-terms and noise-like artifacts in the ambiguity domain show themselves in the TF domain, then seriously obscuring the true TF signature. Fig. 4(b, c) and Fig. 5(b, c) present the windowed Choi-Williams distribution and the windowed Gaussian distribution, respectively. These methods first calculate the STAF, and then build the Choi-Williams kernel and the Gaussian kernel with a predefined window length. The TFDs are obtained by the two-dimensional Fourier transform of the kernel and the STAF product. It is evident that the windowed Choi-Williams distribution and the windowed Gaussian distribution are still influenced by the cross-terms and the noise-like effects caused by the missing samples. The chirp-based kernel gives the best results (see Fig. 4(d) and Fig. 5(d)). By keeping only half of the ambiguity domain where the auto-terms reside, the chirp-based kernel not only efficiently reduces the cross-terms but also mitigates the artifacts caused by missing samples. In particular, the removed area contains the Doppler axis, where the noise-like artifacts always appear. Thus, the noise-like effect of the missing data in the TF domain is largely reduced and the TF signatures are more clearly revealed.

## V. CONCLUSION

This paper has introduced a novel method of designing signal-independent kernels in the ambiguity domain. They operate on windowed signals. The frequency slice at the middle point of the window is obtained by the two-dimensional Fourier transform of the STAF and the kernel product. The proposed methods also give superior results when compared with the traditional kernels both in the case of complete data and in the case of incomplete data. This is because the kernels remove half of the ambiguity plane where the signals auto-terms do not reside. In particular, the removed half includes the Doppler axis, where the noise-like artifacts always appear.

## REFERENCES

[1] P. Flandrin and P. Borgnat, "Time-frequency energy distributions meet compressed sensing," *Signal Processing, IEEE Transactions on*, vol. 58, no. 6, pp. 2974–2982, 2010.

[2] V. C. Chen, "Analysis of radar micro-doppler with time-frequency transform," in *Statistical Signal and Array Processing, 2000. Proceedings of the Tenth IEEE Workshop on*, pp. 463–466, IEEE, 2000.

[3] P. Setlur, M. Amin, and T. Thayaparan, "Micro-doppler signal estimation for vibrating and rotating targets," in *Signal Processing and Its Applications, 2005. Proceedings of the Eighth International Symposium on*, vol. 2, pp. 639–642, IEEE, 2005.

[4] M. Stridh, L. Sörnmo, C. J. Meurling, and S. B. Olsson, "Sequential characterization of atrial tachyarrhythmias based on ecg time-frequency analysis," *Biomedical Engineering, IEEE Transactions on*, vol. 51, no. 1, pp. 100–114, 2004.

[5] I. Christov, G. Gómez-Herrero, V. Krasteva, I. Jekova, A. Gotchev, and K. Egiazarian, "Comparative study of morphological and time-frequency ecg descriptors for heartbeat classification," *Medical engineering & physics*, vol. 28, no. 9, pp. 876–887, 2006.

[6] F. Miwakeichi, E. Martınez-Montes, P. A. Valdés-Sosa, N. Nishiyama, H. Mizuhara, and Y. Yamaguchi, "Decomposing eeg data into space–time–frequency components using parallel factor analysis," *NeuroImage*, vol. 22, no. 3, pp. 1035–1045, 2004.

[7] O. Yilmaz and S. Rickard, "Blind separation of speech mixtures via time-frequency masking," *Signal Processing, IEEE transactions on*, vol. 52, no. 7, pp. 1830–1847, 2004.

[8] Y. T. Nguyen, M. G. Amin, M. Ghogho, and D. McLernon, "Local sparse reconstructions of doppler frequency using chirp atoms," in *Radar Conference (RadarCon), 2015 IEEE*, pp. 1280–1284, IEEE, 2015.

[9] Y. Nguyen, D. McLernon, and M. Ghogho, "Simplified chirp dictionary for time-frequency signature sparse reconstruction of radar returns," in *Compressed Sensing Theory and its Applications to Radar, Sonar and Remote Sensing (CoSeRa), 2016 4th International Workshop on*, pp. 178–182, IEEE, 2016.

[10] H.-I. Choi and W. J. Williams, "Improved time-frequency representation of multicomponent signals using exponential kernels," *IEEE Transactions on Acoustics, Speech, and Signal Processing*, vol. 37, no. 6, pp. 862–871, 1989.

[11] B. Boashash, *Time-frequency signal analysis*. Prentice Hall, 1991.

[12] A. Rihaczek, "Signal energy distribution in time and frequency," *IEEE Transactions on Information Theory*, vol. 14, no. 3, pp. 369–374, 1968.

[13] R. Abeysekera and B. Boashash, "Time-frequency domain features of ecg signals: Their application in p wave detection using the cross wigner-ville distribution," in *Acoustics, Speech, and Signal Processing, 1989. ICASSP-89., 1989 International Conference on*, pp. 1524–1527, IEEE, 1989.

[14] B. Jokanovic and M. Amin, "Reduced interference sparse time-frequency distributions for compressed observations," *IEEE transactions on signal processing*, vol. 63, no. 24, pp. 6698–6709, 2015.

[15] Y. D. Zhang, M. G. Amin, and B. Himed, "Reduced interference time-frequency representations and sparse reconstruction of undersampled data," in *Signal Processing Conference (EUSIPCO), 2013 Proceedings of the 21st European*, pp. 1–5, IEEE, 2013.

[16] R. G. Baraniuk and D. L. Jones, "A radially-gaussian, signal-dependent time-frequency representation," in *Acoustics, Speech, and Signal Processing, 1991. ICASSP-91., 1991 International Conference on*, pp. 3181–3184, IEEE, 1991.

[17] Y. T. Nguyen, M. G. Amin, M. Ghogho, and D. McLernon, "Time-frequency signature sparse reconstruction using chirp dictionary," in *SPIE Sensing Technology+ Applications*, pp. 94840H–94840H, International Society for Optics and Photonics, 2015.